Contents lists available at ScienceDirect

Applied Catalysis B: Environmental

Porous Co$_3$O$_4$/CuO hollow polyhedral nanocages derived from metal-organic frameworks with heterojunctions as efficient photocatalytic water oxidation catalysts

Yan Zhang [a], Jingwei Huang [a], Yong Ding [a,b,*]

[a] State Key Laboratory of Applied Organic Chemistry, Key Laboratory of Nonferrous Metal Chemistry and Resources Utilization of Gansu Province, College of Chemistry and Chemical Engineering, Lanzhou University, Lanzhou 730000, China
[b] State Key Laboratory for Oxo Synthesis and Selective Oxidation, Lanzhou Institute of Chemical Physics, Chinese Academy of Sciences, Lanzhou 730000, China

ARTICLE INFO

ABSTRACT

A novel material of porous Co$_3$O$_4$/CuO hollow polyhedral nanocages (HPNCs) derived-from metal-organic frameworks (MOF) for photocatalytic water oxidation was reported for the first time and the molar ratio of Co/Cu in this kind material was optimized. The Co$_3$O$_4$/CuO HPNCs composites were characterized by multiple experiments (FETEM, HRTEM, SEM, TGA, PXRD, EDX, ICP-AES, BET, XPS) to confirm the structure and the component. A high turnover frequency (TOF) of 4.9×10^{-3} s^{-1} per metal atom was obtained over Co$_3$O$_4$/CuO-3 HPNCs, which is comparable to those published cobalt based catalysts. At the same time, Co$_3$O$_4$/CuO-3 HPNCs showed a maximum oxygen yield of 50% and quantum yield of 49%. This composite of Co$_3$O$_4$/CuO HPNCs containing heterojunctions may enhance the photocatalytic performance of water oxidation.Various characterization methods prove that Co$_3$O$_4$/CuO HPNCs composites are stable and robust heterogeneous photocatalytic catalysts that can be used repeatedly without any loss in activity. According to the experimental results, we speculate that there are two kinds of reaction mechanisms in this light-driven water oxidation system. One mechanism is widely accepted that high valence metal species play a role in the reaction system. The other one is that the heterojunctions of Co$_3$O$_4$/CuO HPNCs make a great contribution to improve the activity of photocatalytic water oxidation. Meanwhile, we put forward a new idea to design a series of metal oxide catalysts with heterojunctions derived from MOF for light-driven water oxidation.

© 2016 Elsevier B.V. All rights reserved.

1. Introduction

The development of the transformation from solar energy into chemical energy with an efficient, low-cost and practicable route remains a long-term challenge with great promise. Inspired by natural photosynthesis, artificial photosynthesis system, which is optimized by (i) efficient capturing of sunlight, (ii) effective separation of photo-induced electrons and holes, (iii) rapid injection of excited electrons and holes with minimal recombination, and (iv) extensive enhancement of catalytic efficiency for water splitting, attracts broad attention. Moreover, water oxidation is a rate-controlling step in solar-to-chemical energy conversion ascribed to the intrinsic difficulty in multiple-electrons transfer and sluggish kinetics of the subsequent oxygen evolution [1–5]. For this matter, remarkable efforts have been committed to explore different types of inexpensive and efficient water oxidation catalysts (WOC) such as first-row transition metal oxides including cobalt oxides [6–18], iron oxides [19–23], nickel oxides [24–26] and manganese oxides [27–32].

Metal-organic frameworks (MOFs) synthesized by assembling inorganic components (metal clusters or metal ions) with organic components (organic ligands or organometallic complexes) into supermoleculars is an emerging class of porous materials with the natures of chemical adjustability, tunable porosities and miscellaneous functionalities [4,33–35]. Motivated by their aforementioned properties, MOFs have recently been attracted ultrahigh

---

interest for acting as self-sacrificial templates to synthesize porous transition metal oxides, such as Fe_2O_3 [36] Co_3O_4 [37] and Cu_xO [38]. Compared to other templated-strategies, the MOFs-derived metal oxides often manifest peculiar structural features, such as large surface area and hierarchical pore sizes [33,39,40]. In despite of many reports on MOFs-derived metal oxide composites and their applications [41,42], this emerging area is distinguished by momentous challenges. For instance, the rational design to fabricate multiple transition metal oxide with nonspherical hollow interiors remains in its infancy, possibly due to high residual stress induced by combining materials with unique physicochemical properties [42–46].

Here, for the first time, we reported a novel kind of porous Co_3O_4/CuO hollow polyhedral nanocages (HPNCs) materials derived from MOF with heterojunctions to enhance charge separation by an internal electric field, which improves the photocatalytic O_2 evolution activity. The effect of Co/Cu molar ratio in porous Co_3O_4/CuO HPNCs on the photocatalytic water oxidation was discussed in detail. The sample of Co_3O_4/CuO-3 HPNCs afforded a high turnover frequency (TOF) of $4.9 \times 10^{-3} s^{-1}$ per metal atom, a maximum oxygen yield of 50% and quantum yield of 49% in this photocatalytic water oxidation system. Numerous characterization experimental results (e.g. XRD, SEM and XPS) confirm that Co_3O_4/CuO-3 HPNCs is extremely stable heterogeneous catalyst. This study proposes a new idea to design a series of metal oxide catalysts with heterojunctions derived from MOF for light-driven water oxidation.

2. Experimental section

2.1. Materials and reagents

All chemicals were of analytical grade and used without purification. $H_2^{18}O$ (97% ^{18}O) was purchased from MASHALL ISOTOPES LTD. Purified water for the preparation of solutions was obtained from a Molecular Lab Water Purifier.

2.2. Synthesis of Co_3O_4/CuO hollow polyhedral nanocages

ZIF-67 was synthesized according to the report by Jiao [47]. Typically, 328.0 mg (4.0 mmol) of 2-methylimidazole were dissolved in 25.0 mL methanol, the solution was poured into the pink solution containing 249.0 mg (1.0 mmol) of cobalt nitrate hexahydrate and 25 mL methanol under stirring with a magnetic bar. Stirring was stopped after combining the component solutions. After aged for 24 h, a purple solid was collected by centrifugation, washed with methanol and dried at room-temperature.

Taking Co_3O_4/CuO-1 HPNCs for example, in total, 240 mg of ZIF-67 templates was first dispersed in 150 mL of ethanol. 36 mg of $Cu(NO_3)_2\cdot6H_2O$ was added into the former solution and the obtained solution was refluxed for 3 h. ZIF-67/Cu HD-1 were collected by centrifugation and finally dried at 60 °C for 12 h. Then, the Co_3O_4/CuO-1 were obtained by annealing the as-obtained ZIF-67/Cu HD-1 particles in air at 360 °C for 2 h with a ramp rate of 2 °C min^{-1}. The amount of added $Cu(NO_3)_2\cdot6H_2O$ to generate Co_3O_4/CuO-2 HPNCs, Co_3O_4/CuO-3 HPNCs and Co_3O_4/CuO-4 HPNCs is 73 mg, 109 mg and 145 mg, respectively.

2.3. Materials characterization

Thermogravimetric analysis (TGA) data were recorded on a NETZSCH STA 449F3 between 25 and 600 °C, with a heating rate 10 °C min^{-1}. Powder X-ray diffraction (PXRD) data were conducted on a PANalytical X'Pert Pro Diffractometer operating at a voltage of 40 kV and a current of 40 mA with Cu Ka radiation ($\lambda = 1.5418$ Å) from 5 to 90(2θ). Specific surface areas were calculated from the N_2 physisorption data obtained at 77 K (Micromeritics ASAP 2020 M system) by using the BJH (Barrett–Joyner–Halenda) and BET methods. Field emission scanning electron microscopy (FESEM) observations were gathered on a Hitachi S-4800 microscope performing at an accelerating voltage of 20.0 kV. Transmission electron microscopy (TEM) images were collected with a JEOL JEM-2010 instrument operating at 200 kV. The GC–MS spectral analysis of isotope labeled O_2 was operated on an Agilent Series 7890A model chromatograph interfaced with an Agilent Series 5975C model mass spectrometer. X-ray photoelectron spectroscopy (XPS) spectra were acquired using an ESCALab220i-XL electron spectrometer.

2.4. Photocatalytic water oxidation

Photocatalytic water oxidation was investigated using a sacrificial system made of $[Ru(bpy)_3]^{2+}$ (1 mM), $Na_2S_2O_8$ (5 mM) and 0.2 g L^{-1} catalyst in 10 mL of borate buffer (pH 8.0, 80 mM). The above solution was deaerated by purging with Ar gas for 10 min in a glass reactor (24 mL) sealed with a rubber septum (the total volume of the reaction solution was 10 mL). The reaction was then started by irradiating the solution with a LED light source (light intensity 16 mW, and beam diameter 2 cm) through a transmitting glass filter ($\lambda \geq 420$ nm) at room temperature. After each sampling time, 100 μL of Ar was injected into the bottle and then the same volume of the gas sample in the headspace of the bottle was taken out by using a SGE gas-tight syringe and analyzed by gas chromatography (GC). The isotope-labeled experiment was performed by repeating the experiment under similar conditions. The 10.8 atom% $H_2^{18}O$ of borate buffer (pH 8.0, 80 mM) containing Co_3O_4/CuO HPNCs (0.2 g L^{-1}), $[Ru(bpy)_3]Cl_2$ (1.0 mM), and $Na_2S_2O_8$ (5.0 mM) was deaerated with helium gas before irradiation by LED light ($\lambda \geq 420$) in a flask sealed with a rubber septum. After irradiation for 30 min, the resulting values of m/z 32 ($^{16}O^{16}O$), 34 ($^{16}O^{18}O$) and 36 ($^{18}O^{18}O$) were monitored systematically by GC–MS. The photocatalytic water oxidation conducted as semiconductor model was performed as following, 0.01 g of Co_3O_4/CuO-3 HPNCs was dispersed in 10 mL of aqueous $NaIO_3$ solution (10 mM) unless otherwise stated.

3. Results and discussion

3.1. Synthesis and characterization

As depicted in Fig. 1, zeolitic imidazolate framework-67 (ZIF-67) single crystals with polyhedron morphology were employed as both precursor and self-sacrificing template to obtain ZIF-67/Cu hydroxide (HD) polyhedron. After calcinations in air for 2 h, porous Co_3O_4/CuO hollow polyhedral nanocages (HPNCs) were synthesized.

ZIF-67 purple solution can be obtained by mixing 2-methylimidazole and cobalt nitrate in methanol with the mixture being aged under ambient conditions for 24 h. As demonstrated in field emission scanning electron microscopy (FESEM), ZIF-67 single crystal has a size approximately 200 nm with smooth surface and defined polyhedral structure (Fig. S1a). The measured powder X-ray diffraction (PXRD) pattern of as-synthesized ZIF-67 corresponds well to the simulated pattern based on the widely accepted geometrical and crystal structural models of ZIF-67 [48] (Fig. S1b).

In the following step, these ZIF-67 particles were dispersed in ethanol solution containing $Cu(NO_3)_2$ and refluxed for 3 h to produce ZIF-67/Cu HD with Cu HD on the surface of precursor ZIF-67. During the process, protons generated from the hydrolysis of Cu^{2+} ions gradually etch ZIF-67 templates and release Co^{2+} ions. Because of the different solubility products of Co^{2+} and Cu^{2+}, Cu^{2+} firstly coordinates with OH$^-$ on the outside of ZIF-67 to form ZIF-67/Cu
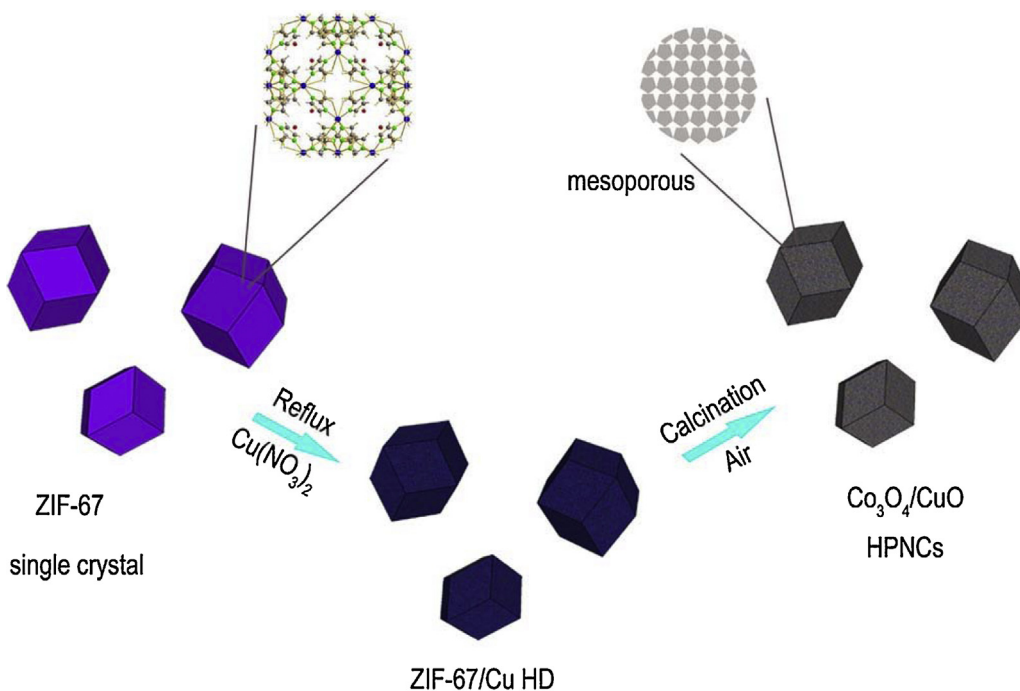
Fig. 1. Schematic illustration for the preparation process of Co_3O_4/CuO hollow polyhedral nanocages (HPNCs).

HD, which was evidenced by the discolourization of original purple solution and appearance of bluish violet precipitation [42,47]. The measured PXRD patterns of as-synthesized ZIF-67/Cu HD (Fig. S2) are consistent almost with the simulated pattern of ZIF-67. The SEM images of ZIF-67/Cu HD (Fig. 2a, c, e and g) show that the materials keep the original polyhedron morphology. With the increasing amount of $Cu(NO_3)_2$, a new flake compound containing copper formed in ZIF-67/Cu HD-4.

The as-prepared ZIF-67/Cu HD was further transformed into the porous Co_3O_4/CuO hollow polyhedral nanocages at 360 °C in air atmosphere at a heating rate 2 °Cmin^{-1}. As confirmed by the thermogravimetric analysis (TG) (Fig. S3), after the initial loss (~2 wt.%) of adsorbed and coordinated water molecules, a steep weight loss (~59.1 wt%) was observed beyond ~200 °C due to decomposition of ZIF-67/Cu HD. Hence, annealing the as-prepared ZIF-67/Cu HD at 360 °C in air flow for 2 h is sufficient to ensure complete conversion from ZIF-67/Cu HD to Co_3O_4/CuO HPNCs. At the same time, the nitrogen peak in the EDX spectra of the four Co_3O_4/CuO HPNCs materials (Fig. S4) is absent, indicating the complete oxidation from ZIF-67/Cu HD to Co_3O_4/CuO HPNCs.

The presence of metal elements and the quantification of the metal elements ratio in the materials were acquired by Inductively Coupled Plasma Atomic Emission Spectroscopy (ICP-AES) (Table S1). With the ordinal number of the samples increasing, the contents of Cu in the final calcined catalysts show the increasing tendency as the original input for the precursors. The images of FESEM (Fig. 2b, d, f and h) and TEM (Fig. 3) reveal that structures of the obtained Co_3O_4/CuO HPNCs are porous and hollow polyhedral nanocages constituted by individual nanoparticles. The formation of nanoparticles and porous surface is resulted from the release of gas molecules during calcination and recrystallization process. Furthermore, the lattice fringes can be clearly seen in the high-resolution transmission electron microscopy (HRTEM) images (Fig. 3) of the obtained Co_3O_4/CuO HPNCs. Among them, the image of Co_3O_4/CuO-4 HPNCs is not clear because the strong magnetism of it leads to image drift. In the case of Co_3O_4/CuO-3 HPNCs, 0.46 nm, 0.28 nm and 0.24 nm can be assigned to the (111), (220) and (311) interlayer spacing of Co_3O_4, respectively. While

0.25 nm and 0.23 nm matches well with the spacing of the (11-1) and (111) planes of CuO, respectively. Interfaces in Co_3O_4/CuO samples can be observed and were marked as red tag area (Fig. 3a3–c3). The TEM and HRTEM images of Co_3O_4/CuO-1 HPNCs, Co_3O_4/CuO-2 HPNCs and Co_3O_4/CuO-4 HPNCs demonstrate the similar morphology and structure with that of Co_3O_4/CuO-3 HPNCs. Moreover, the well-defined rings of selected-area electron diffraction (SAED) patterns can be indexed to various crystalline planes, confirming the polycrystallinity of all Co_3O_4/CuO HPNCs materials (Fig. 3). In addition, the spatial distribution of different elements in Co_3O_4/CuO-3 HPNCs is investigated by elemental mapping analysis on a representative Co_3O_4/CuO-3 HPNCs sample using TEM observation. The elemental mapping results indicate that Co, Cu and O (Fig. 4) are distributed homogeneously within the HPNCs structure. The crystallinity and co-existence of two kinds of metal oxides are further confirmed by PXRD shown in Fig. 5a. The diffraction peaks can be indexed to cubic Co_3O_4 (JCPDS#42-1467, space group Fd3m) and monoclinic CuO (JCPDS#48-1548, space group C2/c). No peaks for the precursor were observed in the XRD patterns. With the ordinal number of the four samples increasing, the intensity of the diffraction peaks for CuO increases, consistent with the results of ICP-AES.

The detailed element chemical states of these Co_3O_4/CuO HPNCs were further characterized by XPS measurements. In the high-resolution XPS spectra (Fig. 5) for Co_3O_4/CuO-3 HPNCs, the Co 2p spectrum (Fig. 5b) presents a broad Co 2p$_{3/2}$ peak at ~779.7 eV and a Co 2p$_{1/2}$ peak at ~794.8 eV. The spin–orbit splitting is 15.1 eV, which indicates the coexistence of the Co(II) and Co(III) [8,14,49]. The Cu 2p spectrum (Fig. 5c) of Co_3O_4/CuO-3 HPNCs shows one spin-orbit doublet Cu 2p$_{1/2}$ peak at ~953.7 eV with a satellite peak at ~962.2 eV and the other spin-orbit doublet Cu 2p$_{3/2}$ peak at ~934.0 eV with two satellites peaks at ~941.3 and ~943.7 eV that correspond to Cu^{2+} state for the Cu atoms [50,51]. The O 1 s spectrum of Co_3O_4/CuO-3 HPNCs exhibits two oxygen bonding features (Fig. 5d). The peaks at ~530.0 eV is typical of the metal-oxygen bond of Co_3O_4 and CuO [8,49–51]. The peak at ~531.4 eV is commonly associated with OH$^-$ belonging to the defect-oxide or hydroxyl-like group [52,53]. For Co_3O_4/CuO-1 HPNCs, Co_3O_4/CuO-2 HPNCs
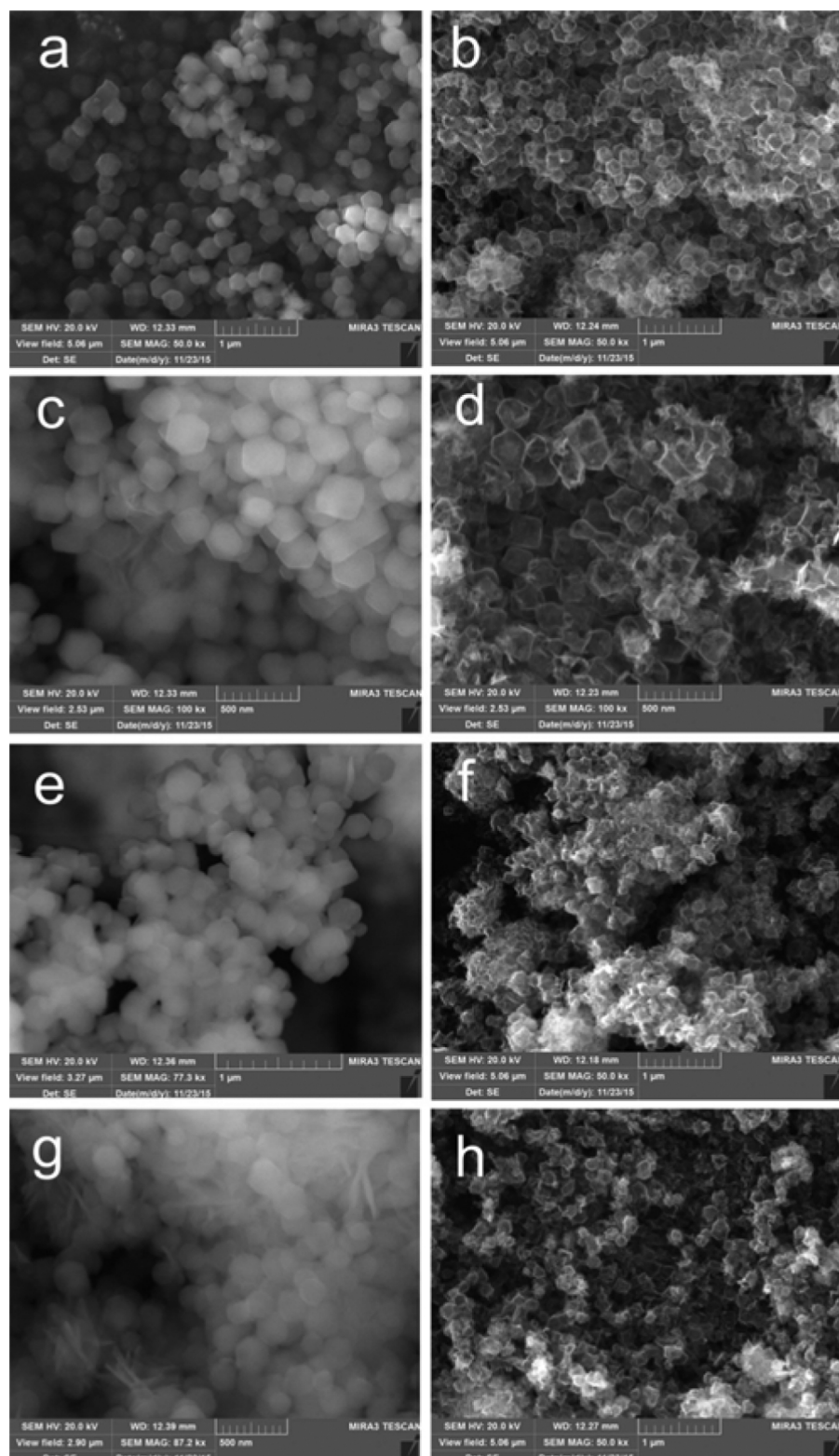
Fig. 2. FESEM images of (a) ZIF-67/Cu HD-1 (b) Co_3O_4/CuO-1 HPNCs (c) ZIF-67/Cu HD-2 (d) Co_3O_4/CuO-2 HPNCs (e) ZIF-67/Cu HD-3 (f) Co_3O_4/CuO-3 HPNCs (g) ZIF-67/Cu HD-4 and (h) Co_3O_4/CuO-4 HPNCs.

and Co_3O_4/CuO-4 HPNCs, we found similar results. With the ordinal number of samples increasing, the XPS peak intensity of Cu increases consistently with the ratio law of Cu/Co in the four materials. Taken together, these results show that these Co_3O_4/CuO HPNCs contain Co^{2+}, Co^{3+}, Cu^{2+} and O^{2-}.

Brunauer-Emmett-Teller (BET) surface area data of these Co_3O_4/CuO HPNCs materials are shown in Table S1. As shown in Fig. S5, all Co_3O_4/CuO HPNCs samples have a type IV isotherm that is characteristic for mesoporous materials. It is universally accepted that there is a correlation between the shape of hysteresis loop and texture of the materials. In addition, the hysteresis loops of
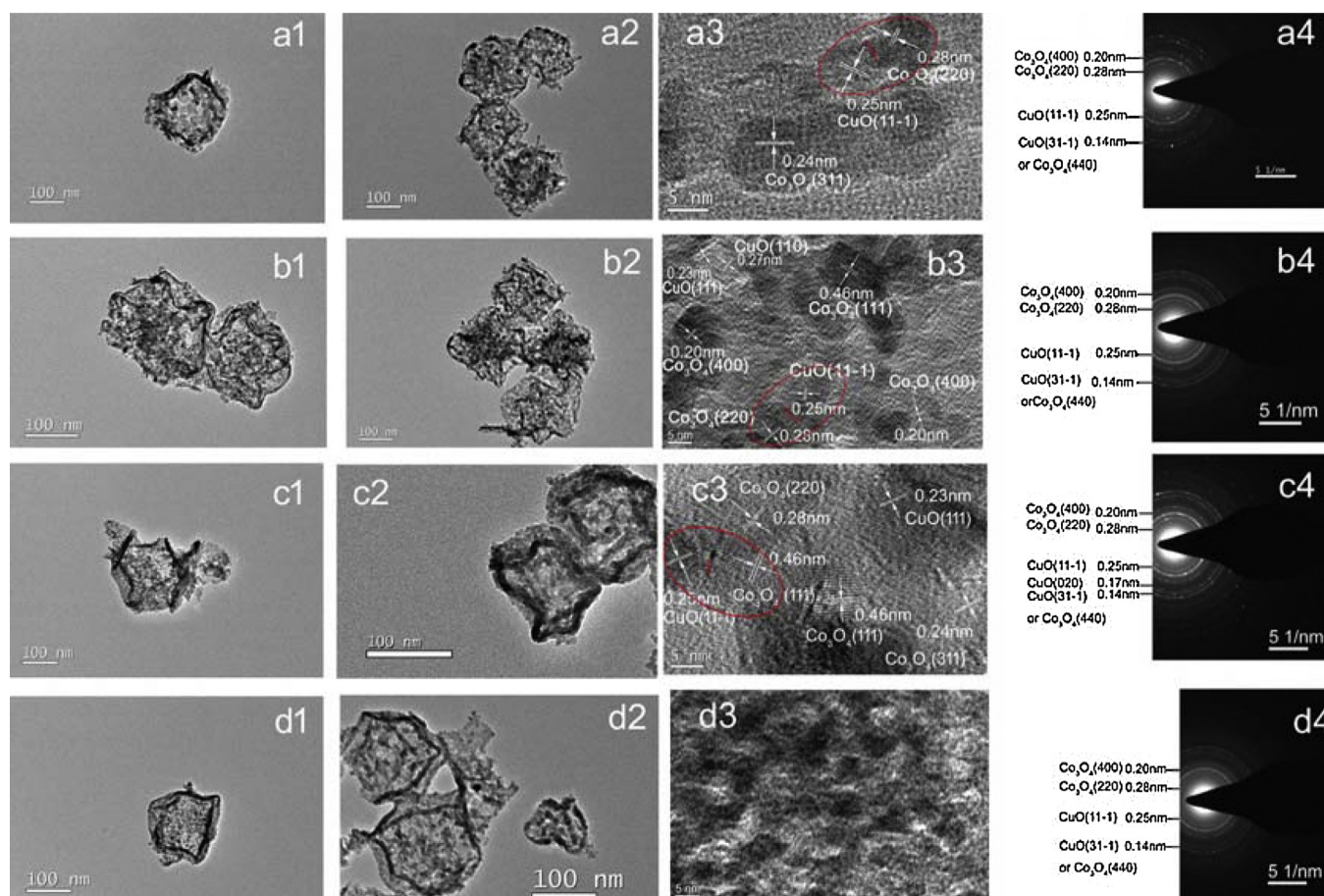
Fig. 3. Structure characterization of (a) Co_3O_4/CuO-1 HPNCs, (b) Co_3O_4/CuO-2 HPNCs (c) Co_3O_4/CuO-3 HPNCs and (d) Co_3O_4/CuO-4 HPNCs. (1) (2) TEM images. (3) HRTEM images. (4) SAED patterns. Scale bars, 5 nm in parts a3–d3; 100 nm in parts a1–d1, a2–d2.

Co_3O_4/CuO 1–4 HPNCs are H3, which is typically associated with the open ends of the wedges. It illustrates that the structures of Co_3O_4/CuO 1–4 HPNCs are almost similar [14,54]. While there are some differences about the pore size distributions of the materials as shown in Fig. S5 inset. Co_3O_4/CuO-1 and Co_3O_4/CuO-2 have a monomial distribution with a wide pore centered at 28 nm [14], which can be attributed to the internal cavities of the nanocages. Co_3O_4/CuO-3 and Co_3O_4/CuO-4 show a bimodal distribution with a narrow distribution centered at about 10 nm and a wide distribution centered at 31 nm. These values correspond to the mesoporous walls of the nanocages and the internal cavities of the nanocages, respectively. It is expected that this porous 3D hollow architecture offer abundant active sites [55].

3.2. Photochemical water oxidation

The photocatalytic activity of these Co_3O_4/CuO HPNCs for water oxidation was investigated in the presence of two-electron acceptor ($Na_2S_2O_8$) and photosensitizer ($[Ru(bpy)_3]^{2+}$) in a close to neutral pH borate buffer solution (pH 8.0). The overall photocatalytic water oxidation cycle is shown in Fig. 6, in which $Na_2S_2O_8$ reacts with the $[Ru(bpy)_3]^{2+*}$ (photoexcited state of $[Ru(bpy)_3]^{2+}$) to form $[Ru(bpy)_3]^{3+}$, sulfate radical and sulfate. The sulfate radical with a potential of 2.4 V vs. NHE will react with the additional $[Ru(bpy)_3]^{2+}$ in solution to form another equivalent of $[Ru(bpy)_3]^{3+}$. The generated $[Ru(bpy)_3]^{3+}$ can oxidize water into oxygen in the presence of WOCs [56,57].

To corroborate that the oxygen is generated from water, the oxidation reaction was performed in 10.8 atom% $H_2{}^{18}O$ of borate buffer (pH 8.0, 80 mM) (Fig. S6). The considerable agreement between the experimental and calculated values of the isotopic ratio for the generated dioxygen clearly testifies that the source of oxygen atoms is water.

The results of photocatalytic water oxidation catalyzed by various Co_3O_4/CuO HPNCs, Co_3O_4 HPNCs, simple metal oxides and control experimental data were shown in Fig. 7. Several control experiments that involve the absence of $Na_2S_2O_8$, $[Ru(bpy)_3]^{2+}$ and catalyst were performed, and a few amounts or no O_2 evolution were detected. The results demonstrated that each of these ingredients is essential in the visible-light-driven water oxidation system. All Co_3O_4/CuO HPNCs materials show obvious catalytic activities for visible-light irradiation water oxidation. The amount of O_2 evolved over Co_3O_4/CuO-3 HPNCs obtained after 11 min photoirradiation was 12.44 μmol, which was remarkably larger than those obtained with Co_3O_4/CuO-1 HPNCs (7.65 μmol), Co_3O_4/CuO-2 HPNCs (9.83 μmol) and Co_3O_4/CuO-4 HPNCs (11.38 μmol). The oxygen yields of Co_3O_4/CuO 1–4 HPNCs were measured to be 31%, 40%, 50% and 45%, respectively. The Quantum yield of the best catalyst Co_3O_4/CuO-3 HPNCs is 49%. The oxygen amounts over all Co_3O_4/CuO HPNCs catalysts have been normalized to per mole of transition metal (Table 1) because only transition metals are participated in the water oxidation process. After 1 min photoirradiation, the TOF of 4.9×10^{-3} mol_{O2} mol_{metal}^{-1} s^{-1} obtained from Co_3O_4/CuO-3 HPNCs was obviously higher than those of Co_3O_4/CuO-1 HPNCs (2.5×10^{-3} mol_{O2} mol_{metal}^{-1} s^{-1}), Co_3O_4/CuO-2 HPNCs (2.9×10^{-3} mol_{O2} mol_{metal}^{-1} s^{-1}) and Co_3O_4/CuO-4 HPNCs (3.4×10^{-3} mol_{O2} mol_{metal}^{-1} s^{-1}). The values obtained here for Co_3O_4/CuO HPNCs are comparable to
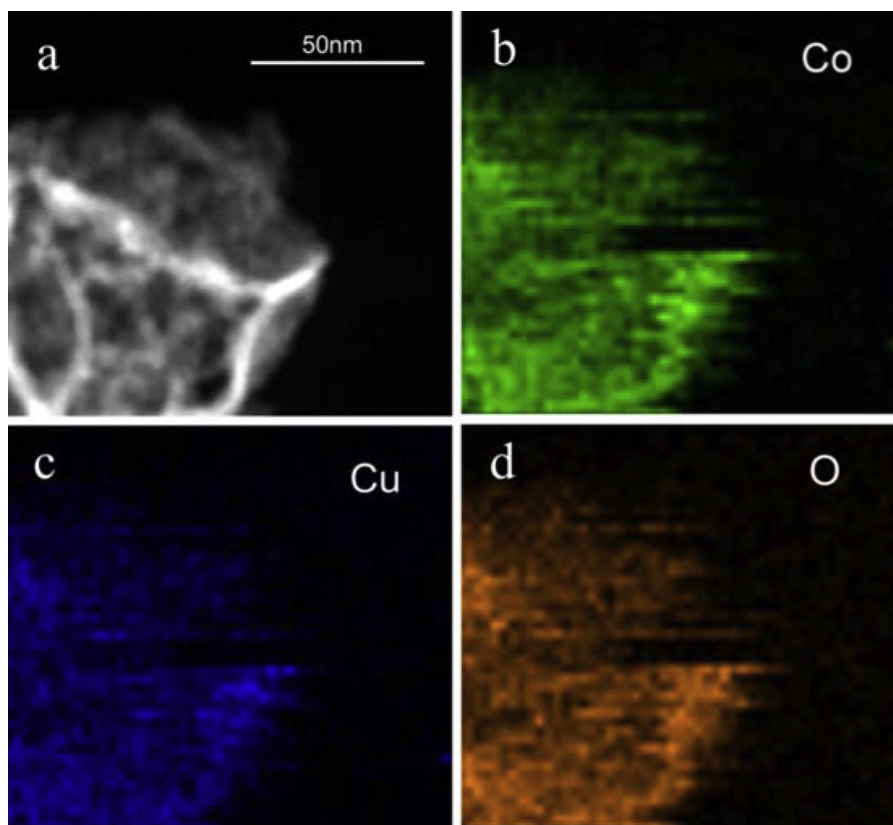
Fig. 4. Elemental mapping of the Co_3O_4/CuO-3 HPNCs. (a) TEM image of an individual Co_3O_4/CuO-3 HPNCs and elemental mapping of Co (b), Cu (c) and O (d).

Table 1
Summary of the photocatalytic water oxidation catalyzed by Co_3O_4/CuO HPNCs.

Catalyst	TOF[a] (mol_{O2} mol_{metal}^{-1} s^{-1})	TOF[b] (μmol_{O2} s^{-1} m^{-2})
Co_3O_4/CuO-1 HPNCs	2.6×10^{-3}	0.53
Co_3O_4/CuO-2 HPNCs	2.9×10^{-3}	0.55
Co_3O_4/CuO-3 HPNCs	4.9×10^{-3}	0.89
Co_3O_4/CuO-4 HPNCs	3.4×10^{-3}	0.76
Co_3O_4 HPNCs[c]	2.1×10^{-3}	0.47

[a] The turnover frequencies (TOFs) per metal ion were calculated for the first 60 s ($TOF = TON/60$ s, TON = mol of oxygen produced in 1 min mol^{-1}).

[b] The apparent turnover frequencies (TOFs) were normalized by using BET surface areas at 1 min after photoirradiation.

[c] Co_3O_4 HPNCs was obtained by calcination of ZIF-67.

those reported Co-based heterogeneous water oxidation catalysts (Table S2). The catalytic activities of Co_3O_4/CuO HPNCs catalysts were also evaluated by the apparent turnover frequencies (TOFs) (Table 1.). The apparent TOFs were normalized by BET surface areas after 1 min photoirradiation. The sample of Co_3O_4/CuO HPNCs-3 exhibits an apparent TOF of 0.89 μmol $s^{-1} m^{-2}$, which is higher than those of Co_3O_4/CuO-1 (0.53 μmol $s^{-1} m^{-2}$), Co_3O_4/CuO-2 HPNCs(0.55 μmol s^{-1} m^{-2})and Co_3O_4/CuO-4 HPNCs (0.76 μmol s^{-1} m^{-2}). Moreover, the activities of Co_3O_4/CuO HPNCs for water oxidation are higher than Co_3O_4 HPNCs obtained by calcination of ZIF-67.

Commercial Co_3O_4, CuO and the mixture of Co_3O_4 and CuO with the same Co/Cu ratio of Co_3O_4/CuO-3 were investigated under the same photocatalytic condition (Fig. 7). The three catalysts without heterojunctions show similar activities with a little difference and the activity sequence is commercial Co_3O_4> the mixture of Co_3O_4 and CuO> commercial CuO. As reported before, the active intermediate would be species (Co or Cu) with high metal valence state during the photocatalytic water oxidation for these simple metal oxides [11,58–60]. The addition of CuO to Co_3O_4 only with

mechanical mixing did not improve the catalytic activities (Fig. 7). The activity fluctuations of commercial metal oxides are different from that of Co_3O_4/CuO HPNCs.

Based on the experimental results, we speculated that there were two kinds of reaction mechanism in this light-driven water oxidation system. One mechanism is widely accepted that high metal valence state species play a role during the reaction process [11,58–60]. The other one is that the heterojunctions formed in Co_3O_4/CuO HPNCs make a great contribution to the good activities of photocatalytic water oxidation. In the visible-light driven water oxidation system, both Co_3O_4 and CuO could absorb visible light to produce photoinduced electron–hole pairs. Since Co_3O_4 and CuO are p-type semiconductors, a large number of nanoscale p–p junctions could be generated when two such types of semiconductor materials are closely attached (Fig. 8) [43,61–64]. It has been calculated that the conduction band (CB) position Co_3O_4 (0.31 eV vs. NHE pH = 8) is lower than that of CuO (0.49 eV vs. NHE pH = 8) [61,65]. The detailed calculation process is in Table S3. Therefore, the photo-induced electrons on the CB of Co_3O_4 can directly transfer to the CB of CuO, then they will reduce $[Ru(bpy)_3]^{3+}$ to $[Ru(bpy)_3]^{2+}$ for the following circular reaction and simultaneously reduce the recombination process of electron–hole pairs. As for the valence band (VB), the corresponding VB position of Co_3O_4 (2.38 eV vs. NHE pH = 8) is higher than that of CuO (2.19 eV vs. NHE pH = 8). As a result, the photogenerated holes on the VB of Co_3O_4 can migrate to the VB of CuO. The holes from Co_3O_4 together with the holes excited from the VB of CuO, would transfer to the surface of CuO to oxidize H_2O to O_2. Therefore, the synergetic enhancement of surface reaction kinetics and bulk charge separation is successfully achieved by the nanoscale heterojunctions with an internal electric field in Co_3O_4/CuO HPNCs, which would improve the photocatalytic O_2 evolution activity [66]. From the activities measurements of the four Co_3O_4/CuO HPNCs samples, it was found that an appropriate
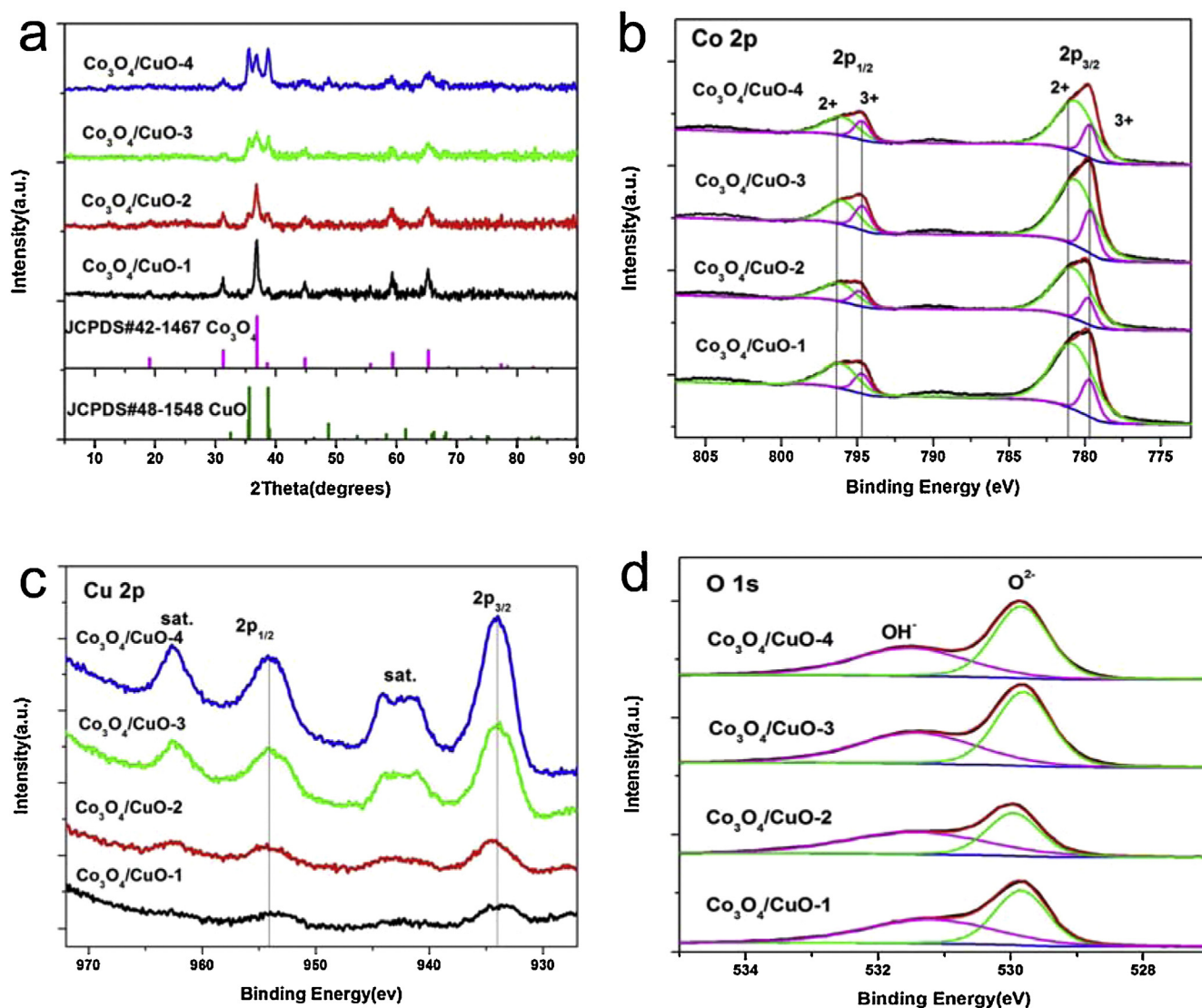
Fig. 5. Characteristics of the as-prepared Co_3O_4/CuO HPNCs. (a) PXRD patterns. (b-d) high-resolution XPS spectra of Co 2p, Cu 2p, and O 1s, respectively.

amount of CuO can significantly enhance the photocatalytic activity for O_2 evolution. The activity for water oxidation initially increased and then decreased with increasing amounts of CuO in the four Co_3O_4/CuO HPNCs samples. The reason may be that in sample of Co_3O_4/CuO-4 HPNCs, the excessive CuO cannot efficiently contact with Co_3O_4 to form heterojunctions, which will result in the reduce of activity for water oxidation.

To demonstrate the aforementioned inference, we conducted the following experiments. Firstly, Co_3O_4 HPNCs with similar morphology and specific surface area of Co_3O_4/CuO HPNCs obtained by calcination of ZIF-67 (Fig. S7) was tested in this photocatalytic water oxidation system. The activity of Co_3O_4 HPNCs is lower than those of Co_3O_4/CuO HPNCs samples with heterojunctions (see Fig. 7). For Co_3O_4 HPNC sample, only the mechanism of high metal valence state plays a role during the reaction process because no heterojunctions exist in this cobalt oxide cage catalyst. The Co_3O_4/CuO-3 HPNCs samples afforded enhanced oxygen yield (50%) compared with that of Co_3O_4 HPNC sample (24.6%). Therefore, we conclude that not only the mechanism of high metal valence state but also the heterojunctions mechanism exist and work during the photocatalytic water oxidation reaction catalyzed by the composite catalyst

of Co_3O_4/CuO HPNCs. The two functions in the photocatalytic water oxidation over Co_3O_4/CuO HPNCs promoted the improved activities of photocatalytic water oxidation.

Secondly, Co_3O_4/CuO-3 HPNCs are capable of photocatalyzing water oxidation under visible light in the presence of iodate ions (IO_3^-) which act as an electron acceptor under near-neutral pH conditions without the addition of photosensitizer (Fig. S8). The results demonstrate that Co_3O_4/CuO-3 HPNCs as a semiconductor have activity for water oxidation in the presence of electron acceptors. The control experiment without $[Ru(bpy)_3]Cl_2$ was performed, and no O_2 evolution was detected. The result proves that $Na_2S_2O_8$ is not a good electron acceptor for Co_3O_4/CuO-3 HPNCs as a semiconductor catalyst for water oxidation. In the $Na_2S_2O_8/[Ru(bpy)_3]Cl_2$ photocatalytic water oxidation system, $[Ru(bpy)_3]^{3+}$ is probably a better electron acceptor to improve the activity of Co_3O_4/CuO-3 HPNCs for water oxidation, while so far we cannot give a solid and direct evidence. These results demonstrated that the seamlessly integration of Co_3O_4 and CuO to form heterojunctions is essential for efficient photocatalytic water oxidation system and the second catalytic mechanism really exist.
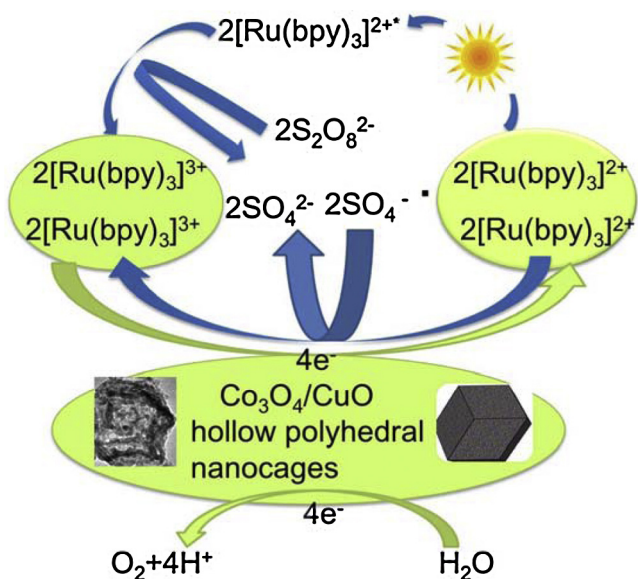
Fig. 6. Photocatalytic water oxidation cycle in the presence of catalyst, photosensitizer and electron acceptor.

Fig. 8. Band diagram and mechanism of charge separation for Co_3O_4/CuO heterojunctions.

3.3. Stability studies of Co_3O_4/CuO HPNCs

The stability of Co_3O_4/CuO-3 HPNCs was first investigated by repetitive water oxidation experiments. As shown in Fig. 9, no significant change in the total amount of O_2 evolution was observed for the five recycling runs. These results indicate that Co_3O_4/CuO-3 HPNCs have excellent activity and stability. In addition, the Co_3O_4/CuO-3 HPNCs catalysts before and after reaction were examined by powder XRD (Fig. 10a) and SEM (Fig. 11) characterizations. No obvious variations in either the powder XRD patterns or the morphology of Co_3O_4/CuO-3 HPNCs were found. The surface conditions of Co_3O_4/CuO-3 HPNCs before and after the photocatalytic reaction were investigated by XPS. Fig. 10b displays the XPS spectra of the Co $2p_{3/2}$ peak at 779.7 eV and the Co $2p_{1/2}$ peak at 794.8 eV for Co_3O_4/CuO-3 HPNCs samples before and after the reaction. The binding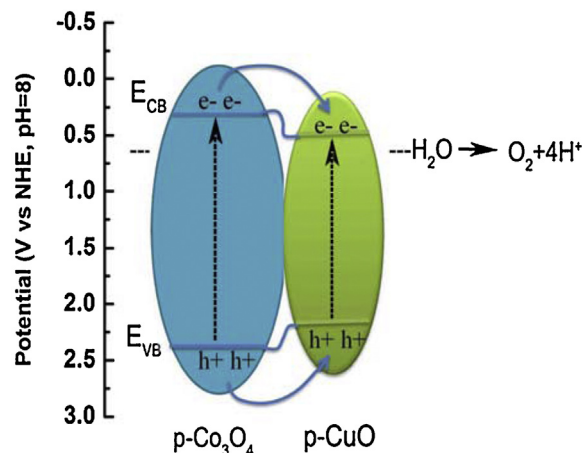 energies of these peaks indicate that the Co species in the samples are Co^{3+} and Co^{2+} by comparison with the Co 2p peak positions of Co_3O_4 [49,53].

The similar intensity ratios and the binding energies of the Co^{2+} and Co^{3+} species for the fresh and used samples indicate that the surface conditions are the same during the photocatalytic water oxidation under highly oxidizing conditions. Fig. 10c displays the XPS spectrum of Cu. For Cu $2p_{3/2}$, one spin-orbit doublet peak is 934.0 eV with two satellite peaks at 941.3 and 943.7 eV before the reaction and that is 934.0 eV with two satellite peaks at 941.2 and 944.6 eV after the reaction. Besides, for the Cu $2p_{1/2}$, one spin-orbit doublet peak is 953.7 eV with a satellite peak at 962.2 eV before the reaction and that is 953.5 eV with a satellite peak at 962.2 eV after the reaction. The same binding energy before and after the reaction assigned to Cu^{2+} strongly indicate that there is no change in the valence state of Cu^{2+} [50,51]. No changes in the surface conditions of Co_3O_4/CuO-3 HPNCs before and after the reaction are also supported by the absence of a shift in the O 1 s peak (Fig. 10d, Fig. S9 survey). Thus, Co_3O_4/CuO-3 HPNCs is highly robust catalyst in the photocatalytic water oxidation.
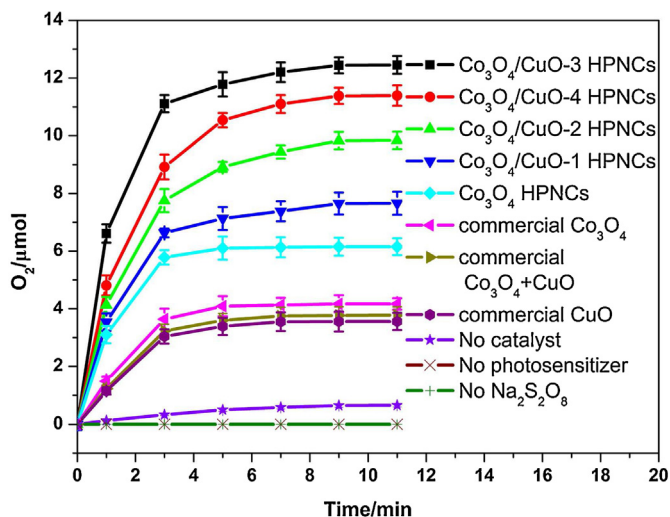

Fig. 7. Time courses of O_2 evolution under photoirradiation (LED lamp, $\lambda \geq 420$ nm Fig. S10) in a NaBi buffer solution (pH 8.0, 10.0 mL) containing $Na_2S_2O_8$ (5.0 mM), $[Ru(bpy)_3]Cl_2$ (1.0 mM) and catalyst (0.20 g L^{-1}) at room temperature. Co_3O_4 HPNCs are obtained by calcination of ZIF-67. The ratios of Co/Cu for the mixture (commercial Co_3O_4 + CuO) and Co_3O_4/CuO-3 HPNCs are the same.

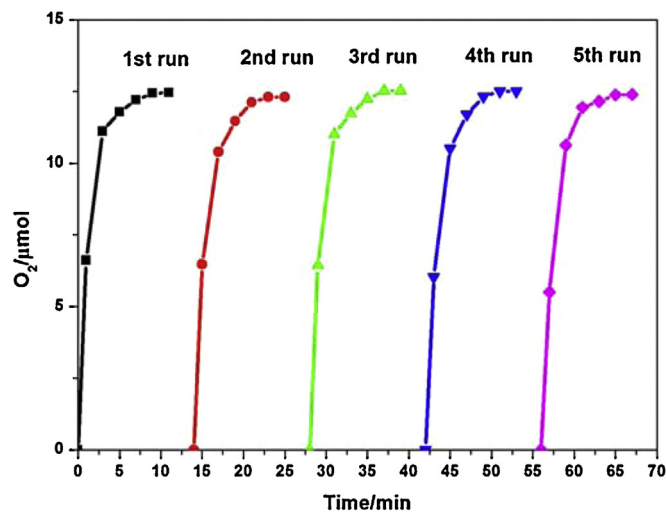**Fig. 9.** Time courses of O_2 evolution of Co_3O_4/CuO-3 HPNCs under photo-irradiation (LED lamp, $\lambda \geq 420$ nm) for five repetitive examination in NaBi buffer solution (pH 8.0, 10.0 mL) containing $Na_2S_2O_8$ (5.0 mM), $[Ru(bpy)_3]Cl_2$ (1.0 mM) and catalyst (0.20 g L^{-1}) at room temperature.

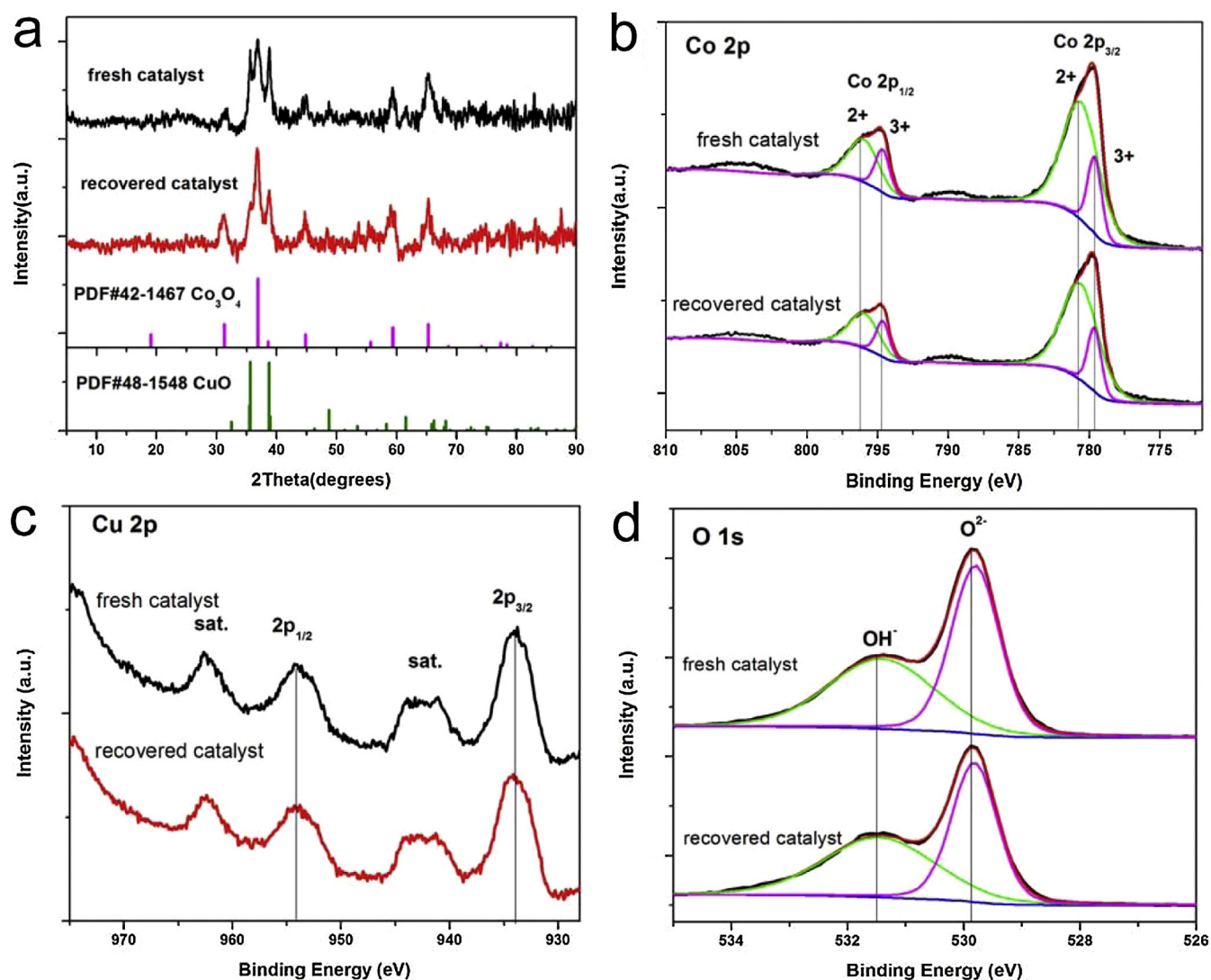**Fig. 10.** XRD patterns (a) and High-resolution XPS spectra (b–d) of fresh Co_3O_4/CuO-3 HPNCs and recovered Co_3O_4/CuO-3 HPNCs.
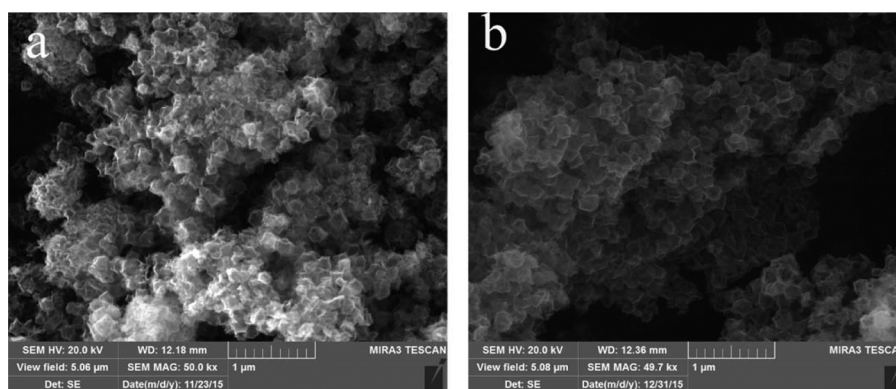
Fig. 11. FESEM images of (a) fresh Co_3O_4/CuO-3 HPNCs and (b) recovered Co_3O_4/CuO-3 HPNCs.

4. Conclusion

In summary, using MOFs as both precursor and sacrificial template, we have demonstrated a facile and controllable synthesis of Co_3O_4/CuO hollow polyhedral nanocages (HPNCs) with the formation of nanoscale heterojunctions for the first time. Furthermore, the ratio of Cu and Co in the Co_3O_4/CuO (HPNCs) was optimized

to obtain the best catalyst for water oxidation. These Co_3O_4/CuO HPNCs materials exhibited superior photocatalytic water oxidation activity with a TOF of $4.9 \times 10^{-3}\,s^{-1}$, an oxygen yield of 50% and a quantum yield of 49%, respectively. The Co_3O_4/CuO HPNCs containing heterojunctions plays a significant role in enhancing charge separation by an internal electric field which improves the photocatalytic O_2 evolution activity in light-drive water oxida-

tion system. Compared with other cobalt-based materials reported, water oxidation performance of our Co_3O_4/CuO hollow polyhedral nanocage materials is excellent. The strategy of utilization precursor opens a new route for preparing porous materials. About all, we believed we put forward a new idea to design a series of metal oxide catalysts with heterojunctions derived from MOF for efficient light-driven water oxidation.

Acknowledgments

Appendix A. Supplementary data

Supplementary data associated with this article can be found, in the online version, at http://dx.doi.org/10.1016/j.apcatb.2016.05.078.

References

[1] K.N. Ferreira, T.M. Iverson, K. Maghlaoui, J. Barber, S. Iwata, Science 303 (2004) 1831–1838.
[2] J. Ryu, S.H. Lee, D.H. Nam, C.B. Park, Adv. Mater. 23 (2011) 1883–1888.
[3] J.H. Kim, M. Lee, J.S. Lee, C.B. Park, Angew. Chem. Int. Ed. 51 (2012) 517–520.
[4] D. Gust, T.A. Moore, A.L. Moore, Accounts. Chem. Res. 42 (2009) 1890–1898.
[5] Q. Yin, J.M. Tan, C. Besson, Y.V. Geletii, D.G. Musaev, A.E. Kuznetsov, Z. Luo, K.I. Hardcastle, C.L. Hill, Science 328 (2010) 342–345.
[6] F. Jiao, H. Frei, Energy Environ. Sci 3 (2010) 1018.
[7] C.-C. Lin, Y. Guo, J. Vela, ACS Catal. 5 (2015) 1037–1044.
[8] P.W. Menezes, A. Indra, D. González-Flores, N.R. Sahraie, I. Zaharieva, M. Schwarze, P. Strasser, H. Dau, M. Driess, ACS Catal. 5 (2015) 2017–2027.
[9] G.P. Gardner, Y.B. Go, D.M. Robinson, P.F. Smith, J. Hadermann, A. Abakumov, M. Greenblatt, G.C. Dismukes, Angew. Chem. Int. Ed. 51 (2012) 1616–1619.
[10] H. Liu, G.R. Patzke, Chem. Asian J. 9 (2014) 2249–2259.
[11] M. Zhang, M. de Respinis, H. Frei, Nat. Chem. 6 (2014) 362–367.
[12] G.S. Hutchings, Y. Zhang, J. Li, B.T. Yonemoto, X. Zhou, K. Zhu, F. Jiao, J. Am. Chem. Soc. 137 (2015) 4223–4229.
[13] M. Risch, F. Ringleb, M. Kohlhoff, P. Bogdanoff, P. Chernev, I. Zaharieva, H. Dau, Energy Environ. Sci. 8 (2015) 661–674.
[14] J. Wei, Y. Feng, Y. Liu, J. Ding, J. Mater, J. Mater Chem. A 3 (2015) 22300–22310.
[15] X. Zou, A. Goswami, T. Asefa, J. Am. Chem. Soc. 135 (2013) 17242–17245.
[16] H. Liu, M. Schilling, M. Yulikov, S. Luber, G.R. Patzke, ACS Catal. 5 (2015) 4994–4999.
[17] C.W. Cady, G. Gardner, Z.O. Maron, M. Retuerto, Y.B. Go, S. Segan, M. Greenblatt, G.C. Dismukes, ACS Catal. 5 (2015) 3403–3410.
[18] Y. Zhao, X. Zhou, Y. Ding, J. Huang, M. Zheng, W. Ye, J. Catal. 338 (2016) 30–37.
[19] D. Hong, Y. Yamada, T. Nagatomi, Y. Takai, S. Fukuzumi, J.Am. Chem. Soc. 134 (2012) 19572–19575.
[20] X.Q. Du, Y. Ding, R. Xiang, X. Xiang, Phys. Chem. Chem. Phys. 17 (2015) 10648–10655.
[21] Y. Feng, J. Wei, Y. Ding, J. Phys. Chem. C 120 (2016) 517–526.
[22] B. Li, M. Li, C. Yao, Y. Shi, D. Ye, J. Wu, D. Zhao, J. Mater. Chem. A 1 (2013) 6742.
[23] J. Huang, Y. Ding, X. Luo, Y. Feng, J. Catal. 333 (2016) 200–206.
[24] J. Huang, G. Hu, Y. Ding, M. Pang, B. Ma, J. Catal. (2016), http://dx.doi.org/10.1016/j.jcat.2016.05.007.
[25] G. Chen, L. Chen, S.M. Ng, T.C. Lau, ChemSusChem 7 (2014) 127–134.
[26] X. Yu, T. Hua, X. Liu, Z. Yan, P. Xu, P. Du, ACS Appl. Mater. Interfaces 6 (2014) 15395–15402.
[27] D.M. Robinson, Y.B. Go, M. Greenblatt, G.C. Dismukes, J. Am. Chem. Soc. 132 (2010) 11467–11469.
[28] R. Pokhrel, M.K. Goetz, S.E. Shaner, X. Wu, S.S. Stahl, J. Am. Chem. Soc. (2015).
[29] C.-H. Kuo, I.M. Mosa, A.S. Poyraz, S. Biswas, A.M. El-Sawy, W. Song, Z. Luo, S.-Y. Chen, J.F. Rusling, J. He, ACS Catal. 5 (2015) 1693–1699.
[30] D.M. Robinson, Y.B. Go, M. Mui, G. Gardner, Z. Zhang, D. Mastrogiovanni, E. Garfunkel, J. Li, M. Greenblatt, G.C. Dismukes, J. Am. Chem. Soc. 135 (2013) 3494–3501.
[31] Y. Meng, W. Song, H. Huang, Z. Ren, S.Y. Chen, S.L. Suib, J. Am. Chem. Soc. 136 (2014) 11452–11464.
[32] D. Jeong, K. Jin, S.E. Jerng, H. Seo, D. Kim, S.H. Nahm, S.H. Kim, K.T. Nam, ACS Catal. (2015) 4624–4628.
[33] F. Zheng, Y. Yang, Q. Chen, Nat. Commun. 5 (2014) 5261.
[34] W. Zhang, G. Lu, C. Cui, Y. Liu, S. Li, W. Yan, C. Xing, Y.R. Chi, Y. Yang, F. Huo, Adv. Mater. 26 (2014) 4056–4060.
[35] R. Banerjee, A. Phan, B. Wang, C. Knobler, H. Furukawa, M. O'Keeffe, O.M. Yaghi, Science 319 (2008) 939–943.
[36] B. Kong, J. Tang, Z. Wu, J. Wei, H. Wu, Y. Wang, G. Zheng, D. Zhao, Angew. Chem. Int. Ed. 53 (2014) 2888–2892.
[37] T.Y. Ma, S. Dai, M. Jaroniec, S.Z. Qiao, J. Am. Chem. Soc. 136 (2014) 13925–13931.
[38] A. Banerjee, U. Singh, V. Aravindan, M. Srinivasan, S. Ogale, Nano Energy 2 (2013) 1158–1163.
[39] Y. Han, P. Qi, S. Li, X. Feng, J. Zhou, H. Li, S. Su, X. Li, B. Wang, Chem. Commun. (Camb.) 50 (2014) 8057–8060.
[40] S. Qiu, M. Xue, G. Zhu, Chem. Soc. Rev. 43 (2014) 6116–6140.
[41] C. Sun, J. Yang, X. Rui, W. Zhang, Q. Yan, P. Chen, F. Huo, W. Huang, X. Dong, J. Mater. Chem. A 3 (2015) 8483–8488.
[42] H. Hu, B. Guan, B. Xia, X.W. Lou, J. Am. Chem. Soc. 137 (2015) 5590–5595.
[43] M.A. Kanjwal, N.A.M. Barakat, F.A. Sheikh, M.S. Khil, H.Y. Kim, J. Mater. Sci. 43 (2008) 5489–5494.
[44] R. Wu, X. Qian, X. Rui, H. Liu, B. Yadian, K. Zhou, J. Wei, Q. Yan, X.Q. Feng, Y. Long, L. Wang, Y. Huang, Small 10 (2014) 1932–1938.
[45] C. Li, T. Chen, W. Xu, X. Lou, L. Pan, Q. Chen, B. Hu, J. Mater. Chem. A 3 (2015) 5585–5591.
[46] J. Shao, Z. Wan, H. Liu, H. Zheng, T. Gao, M. Shen, Q. Qu, H. Zheng, J. Mater. Chem. A 2 (2014) 12194.
[47] Z. Jiang, Z. Li, Z. Qin, H. Sun, X. Jiao, D. Chen, Nanoscale 5 (2013) 11770–11775.
[48] N. Yanai, M. Sindoro, J. Yan, S. Granick, J. Am. Chem. Soc. 135 (2013) 34–37.
[49] J. Li, J. Wang, X. Liang, Z. Zhang, H. Liu, Y. Qian, S. Xiong, ACS Appl. Mater. Interfaces 6 (2014) 24–30.
[50] D.R. Kumar, D. Manoj, J. Santhanalakshmi, J.-J. Shim, Electrochim. Acta 176 (2015) 514–522.
[51] M. Chen, C. Hou, D. Huo, M. Yang, H. Fa, Appl. Surf. Sci. (2015).
[52] F. Jiao, H. Frei, Angew. Chem. Int. Ed. 48 (2009) 1841–1844.
[53] J. Rosen, G.S. Hutchings, F. Jiao, J. Am. Chem. Soc. 135 (2013) 4516–4521.
[54] X. Deng, W.N. Schmidt, H. Tüysüz, Chem. Mater. 26 (2014) 6127–6134.
[55] D. Yang, Z. Lu, X. Rui, X. Huang, H. Li, J. Zhu, W. Zhang, Y.M. Lam, H.H. Hng, H. Zhang, Q. Yan, Angew. Chem. Int. Ed. 53 (2014) 9352–9355.
[56] A.R. Parent, R.H. Crabtree, G.W. Brudvig, Chem. Soc. Rev. 42 (2013) 2247–2252.
[57] Y. Zhao, Y. Zhang, Y. Ding, M. Chen, Dalton Trans. 44 (2015) 15628–15635.
[58] Y. Zhang, J. Rosen, G.S. Hutchings, F. Jiao, Catal. Today 225 (2014) 171–176.
[59] N.S. McCool, D.M. Robinson, J.E. Sheats, G.C. Dismukes, J. Am. Chem. Soc. 133 (2011) 11446–11449.
[60] C. Zhang, A.D. Handoko, Y. Du, S. Xi, B.S. Yeo, ACS Catal. (2016) 2473–2481.
[61] X. Chang, T. Wang, P. Zhang, J. Zhang, A. Li, J. Gong, J. Am. Chem. Soc. 137 (2015) 8356–8359.
[62] X. Guo, P. Diao, D. Xu, S. Huang, Y. Yang, T. Jin, Q. Wu, M. Xiang, M. Zhang, Int. J. Hydrogen Energy 39 (2014) 7686–7696.
[63] P. Chen, T. Zhang, J. Zhang, J. Xiang, H. Yu, S. Wu, X. Lu, G. Wang, F. Wen, Z. Liu, Nanoscale (2016).
[64] Y. Harima, K. Yamashita, J. Phys. Chem. 89 (1985) 5325–5327.
[65] J. Zhang, H. Cui, B. Wang, C. Li, J. Zhai, Q. Li, Appl. Surf. Sci. 300 (2014) 51–57.
[66] Z. Sun, Q. Yue, J. Li, J. Xu, H. Zheng, P. Du, J. Mater. Chem. A 3 (2015) 10243–10247.